# THE TRANSVERSE ACCELERATION INSTABILITY FOR BOW SHOCKS IN THE NONLINEAR REGIME

RUTH DGANI
INTERNET: KNILL@IPAC.CALTECH.EDU
DAVE VAN BUREN
INTERNET: DAVE@IPAC.CALTECH.EDU
AND
ALBERTO NORIEGA-CRESPO
INFRARED PROCESSING AND ANALYSIS CENTER, JET PROPULSION LABORATORY
CALIFORNIA INSTITUTE OF TECHNOLOGY
POSTAL ADDRESS: IPAC, CALTECH 100-22, PASADENA, CA 91125
INTERNET: ALBERTO@IPAC.CALTECH.EDU

## ABSTRACT

We continue our study of the stability of thin isothermal bow shocks. We follow the transverse accelaration instability ( hereafter TAI) found in the linear analysis, to the nonlinear regime. We use numerical simulations to solve the nonlinear Euler equations.

We find that thin isothermal bow shocks are indeed unstable also in the nonlinear regime. The growth rates for the instability are higher for larger values of $v_*/v_w$, as expected from the linear analysis.

We apply our results to observations of bow shocks and obtain that the size of the clumps in $\alpha$ Cam is compatible with the TAI if its viscosity is due to turbulence in the mixing layer between the shocked ambient medium fluid and the shocked wind fluid.

## 1. INTRODUCTION

There are many examples of bow shocks generated by stellar winds. Runaway OB stars traversing the diffuse interstellar medium generate parsec-sized bow shocks (Van Buren and McCray, 1988), examples being $\alpha$ Cam and $\zeta$ Oph. Inside molecular clouds, newly formed OB stars often form cometary compact HII regions, which are well explained as bow shocks (Van Buren *et al.*, 1990; Mac Low *et* ( / / ., 1991). Near the galactic center, where mass losing supergiants interact with the galactic center's wind, a bow shock is seen around IRS 7 (Yusef-Zadeh and Morris 1992, Serabyn, Lacy and Achterman 1992).

The interaction region between the wind and the circumstellar shocked gases is bounded by two shocks in which the flows slow down from supersonic to subsonic velocities. The width of the interaction region depends on the efficiency of the cooling processes as well as on the Mach numbers of the interacting flows. For efficient cooling the interaction zone narrows with increasing Mach number, becoming in the limit infinitesimally thin. The wind velocities of OB stars are $\sim$ 1000 -- 3000 km $s^{-1}$, which lead to very high post-shock temperatures at the wind shock. A variety of' cooling mechanisms are likely to operate, among them turbulent mixing via Kelvin-Helmholz instabilities, thermal con duction and radiation 10 sses, resulting in a narrow interaction region. Studies of the closely related stellar wind bubbles indicate that strong losses can indeed occur (Van Buren 1986).

In an earlier paper (Dgani, Van Buren & Noriega-Crespo 1995; hereafter paper I) we present a linear stability analysis of thin isothermal bow shocks. In that study we follow Soker (1990) and calculate the evolution of shod wavelength perturbations in the zero thickness shell approximation. We find that the motion is unstable in this limit. Moreover, the stability properties depend on one dimensionless parameter $v_*/v_w$ where $v_*$ is the stellar velocity and $v_w$ is the wind velocity. Bow shocks with fast winds for which $v_*$ /vu, << 1 are more stable than bow shocks with slow winds i.e. $v_*/v_w >> 1$. 111 the same paper we compare our results with real bow shocks and find indeed that the IRS 7 bow shock for which $v_*/v_w >> 1$, is more clumpy than bow shocks around runaway OB stars for which $v_*/v_w << 1$.

The instability we found in paper I is of a very similar nature to the colliding wind binary instability described by Dgani, Walder & Nussbaumer (1993) ( see also Dgani 1993, Dgani & Soker 1994). It arises from the fact that density fluctuations in the bow shock surface lead to fluctuations in the transverse acceleration. When the wind stream collides with the ambient medium stream, the shocked slab tends to oscillate away from the equilib-

rium position, accelerated outward by the oblique accretion of the streams, We therefore named this instability in paper I the transverse acceleration instability ('TAI),

Recent high resolution two dimensional numerical calculations of red supergiant bow shocks shows that as the cooling in the shocks increases the shocked region oscillates (Brighenti & D'Ercole 1995). The reason for the instability that appeared in their calculations is not completely clear. It may be related to internal shear motions inside the shell as in the case of Vishniac's nonlinear thin shell instability NTSI ( Vishniac 1994). The high resolution model of Brighenti & D'Ercole for a slow moving star has $v_* / v_w = 2$ while their high resolution model for a fast moving star has $v_* / v_w = 8$. It seems that the cooling model of the slow moving star shown in their Fig. 2 is more stable than the one with the fast mewing star shown in their Fig.3 in accordance with the TAI. However the $v_* / v_w = 2$ model is not thin. In this paper we calculate thin models.

Here we perform pressureless 2D numerical simulations in order to investigate the nonlinear regime of the TAI. In § 2 we present the models. In § 3 we show numerical results and discuss possible applications.

## 2. THE NUMERICAL MODELS

We use the particle in cell (PIC) method to study the bow shock flow. We neglect the pressure, which is equivalent to an isothermal flow with very high Mach number. The PIC numerical method is described in Livio et al. ( 1986) for the Cartesian case. It is adapted to cylindrical coordinates in Dgani & Livio ( 1990). The Eulerian cells in the present case are toroids and the particles are rings about the axis connecting the two stars (see e.g., Harlow 1964). The cylindrical character of the problem is thus retained. The physical variables are calculated at each time step, in each cell, by averaging over the particles residing in that cell. The physical variables of each particle are changed as a result of interaction with all the other particles in the cell. This interaction causes the particles to lose their transverse momentum when they reach the collision surface, even though there is no pressure. The strength of the interaction is determined by two parameters, $\alpha_A$ and $\alpha_B$ (see Livio et al. 1986), which essentially control the local and global averages inside a cell. In all the simulations we have set, $\alpha_B = 1$, which is the maximum due, and $\alpha_A = 0.01$. These parameters are related to the numerical viscosity. The PIC scheme in comparison with elaborate high resolution methods for hydrodynamics, has the advantage of allowing free streaming of particles until they hit the collision surface. The absence of pressure force's is the essence of the isothermal $M = \infty$ flow that we want to investigate in the

nonlinear regime. A similar numerical scheme was used1 to study the nonlinear regime of the instabilities in the Bondi-Hoyle-Lyttleton type accretion flow onto a compact object (Soker 1991) and in the planar colliding wind binary flow (Dgani & Soker 1994).

The geometry of our problem is depicted in Fig. 1 of Paper 1. We define the cylindrical coordinate ($r$, z), centered at the wind source, where z is the coordinate along the symmetry axis and $r$ is the distance from the symmetry axis. We express all quantities in units in which the standoff distance $R_0$, the wind velocity, $v_w$, and the wind density at a standoff distance from the wind source $\rho_0(R_0)$, are taken to be unity.

We present 5 lulls. In model A, the standard model, we assume that $v_* = v_w$. The grid extends from $r = 0.0$ to $r = 2.4$ and from $z = 0.01$ to $z = 1..3$. The cells have equal sizes $\Delta R = \Delta z = 0.02$, and the time step is At = 3.3334. $10^{-3}$. The wind particles are injected from a sphere of radius 0.9 around the wind source in the radial direction from the source. The ambient medium particles are injected from the plane $z = -1.3$ in the $-\hat{z}$ direction. Starting at t=0 with an empty grid we inject 144 wind particles and 144 ambient medium particles at each time st ep.

In model B we increased the number of particles injected per time step by two compared to model A. In model C we increase the cell size, namely $\Delta R = 0.04$. In Models D and E we explore the effects of changing $v_*/v_w$. In Model D we have $v_*/v_w = 2$, and in Model E, $v_*/v_w = 1/2$. The expected difference between models D and E is small (see discussion in section 3). It would be desirable to have larger differences in the ratio $v_*/v_w$, but due to the Courant-Friedrich-Levy condition larger differences in $v_*/v_w$ would require too much computer time and memory. The parameters for the 5 models are presented in Table 1. In the table $N_{inj}$ is the number of particles injected per time step.

## 3. NUMERICAL RESULTS

The initial perturbations in density along the bow shock result from fluctuations in the number of particles in adjacent cells.

In Fig. 2 we present the surface density $\sigma$ of' model A, as a function of the ~~the~~ length coordinate $l$ from $l = 0.1$ to $l = 2$ along the bow shock. The mass variable used in the numerical calculations is related $\sigma r$ and not to $\sigma$ to 01 btain $\sigma$ we devide by the $r$ coordinate. When $l << 1$ $r \ll 1$ and the devision is not well defined. This rerolls in errors for the surface density $\sigma$ near $l = 0$. We therefore show $\sigma$ as a function of $l$ from $l = 0.1$ to $l = 2$. The

first 5 panels are snapshots at 5 different times after the flow is well developed, while in the last panel tile 5 plots are plotted together. It is evident from Fig. 2 that the perturbations grow in size along the bow shock. We show a two dimensional grayscale image in Fig. 3 of' the development of the perturbations with time. The horizental axis represents the coordinate along the bow shock while the vertical coordinate represents the time. The propagation and dispersion of individual perturbations is easy to follow. In our case the perturbation waves move with the fluid velocity ($c_s = 0$). It is clear that in general the perturbations grow as they propagate along the bow shock which can be seen by noting that the contrast between white and black is larger on the right hand side of the figure.

In order to check the effects of the number of particles in the grid on the growth rate of the IIIO(lCS, we use the same grid as in model A, but inject 576 particles per time step in model B instead of 288 particles per time step in model A. As a result the total number of particles in the grid increased from ~320000 to ~640000. The evolution of the surface density $\sigma$ along the bow shock is depicted in Fig. 4, presented at the same time sequence as in Fig. 2. We see that the growth rate is similar to that of model A. This model shows more structure and is less noisy than model A, but the growth rate of the perturbations as well as their dominant length scale are similar in both models.

The change of the cell size effects the growth rate of the surface density perturbations as can be seen in Fig. 5, which shows the surface density for model C, presented at the same time sequence as model A. The perturbation growth in this case is smaller than in model A. This result, is in accordance with the linear analysis, which shows that the growth rate is propotional to the square root of the wave number. In the numerical simulations, the wave number is fixed by the cell sizes and it decreases as the cell sizes increase.

In order to compare between models D and E we recall some of our results in paper I. The perturbation amplitude of a parcel of material flowing from $l_1$ to $l_2$ along the bow shock was shown in paper I to be (Eq. 4.1 in paper I):

$$\log\left[\frac{A(l_2)}{A(l_1)}\right] = \int \frac{Re(i\omega)}{v_{l0}} dl \sim C(l_{ave})((l_2/\lambda)^{1/2} - (l_1/\lambda)^{1/2}) \tag{3.1}$$

where $l_{ave} = (l_1 + l_2)/2$. $C(l)$ is an increasing function of $v_*/v_w$. In Fig. 6 we plot $C$ as a function of $v_*/v_w$ for the angle $\theta = 60^o$ for which 1.-1. Using equation (3.1) and Fig. 6, the amplitude growth for a bow shock with $v_*/v_w = 0.5$ is 1.4 times smaller than that of a bow shock with $v_*/v_w = 2$.

In Fig. 7 we show the relative perturbations in the surface density averaged over time for

models D and E after the flows have been well established. Model D shows larger relative perturbations as expected. The growth of the relative perturbations with $v_*/v_w$ for $l = 1$ which was calculated above is a bit higher than what the two models show. Due to the viscosity in the code the perturbation growth rate for both cases is smaller than the linear growth.

We will now apply the numerical calculations present ed here to runaway OB stars like $\alpha$ Cam. In high resolusion IRAS images of $\alpha$ Cam clumps of the size of 0.1 of the stand off distance $R_0$ appear. We will now use a dimensional argument to show that the size of the clumps in $\alpha$ Cam is compatible wit, h the 'JAI, if its viscosity is due to turbulence in the mixing layer between the shocked ambient medium fluid and the shocked wind fluid.

Under the assumption of isothermal flow the expect ed width of tile bow shock is $\delta \sim M^{-2} R_0$ Where M is the Mach number and $R_0$ is that stand off distance of the bow shock (Van Buren et al. 1990). The turbulent viscosity in the standard mixing length theory (Raga wt al) is of the order of $\nu_t \sim v_t l_t$ where $l_t$ is the size of the largest eddies and $v_t$ is the turbulent velocity. We assume that the tu bulent velocity is of the same order of magni tude as the sound speed because supersoni c turbulent eddies are likely to be dissipated very efficiently (due to the production of shock waves). Taking $l_t$ to be the width of the bow shock $\delta$ we obtain $\nu_t \sim v_* \delta/M$.

The numerical viscosity $\nu_n$ associated with the (PIC) schema is from dimensional considerations of the order of $(\Delta R)^2/\Delta t$ (Soker 1986). $\Delta t$ is bounded by the Courant-Friedrich-Levy condition $\Delta t < \Delta R/v_{max}$ where $v_{max}$ is the maximum velocity in the grid. In our case $v_{max} \approx v_*$ so that $\nu_n \sim$ A $R v_*$. The numerical viscosity is of the same order as the turbulent one if $\Delta R \sim \delta/M$. Our resolution is $\Delta R = 0.02 R_0$ so $\nu_n \sim \nu_t$ for M = 3 relevant for $\alpha$ Cam.

Our models show that the dominant wave length of the perturbations is of the order of $0.1 R_0$ (see Figs 2,3,4). The clumps seen in the bow shock of $\alpha$ Cam have this size. It could be that these clumps result from this instability.

The research described in this paper was carried out by the Jet Propulsion Laboratory, California Institute of Technology, under a contract with the National Aeronautics and Space Administration. R.D. thanks the Swiss National Foundation for its support and the visiting scientist program at ,JPL. AN-C is supported by the NASA Long Term Astrophysics Program.

## References


Brighenti, F., Dercole, A., 1995, MNRAS, in press

Dgani, R., 1993, A&A, 271, 527

Dgani, R., Livio, M., 1990, ApJ, 361, 540

Dgani, IL, & Soker, N., 1994, A&A, 282, 54

Dgani, R., Walder, R.,& Nussbaumer, H., 1993, A&A, 267, 155

Dgani, R.., Van Buren, D., Noriega-Crespo, A., 1995, ApJ (submitted) Paper I

Harlow, F.H., 1964, Method.Comp ut.Phys., 3, 319

Livio, M., Soker, N., de Kool, M., Savonije, G.J., 1986, MNRAS, 218, 593

Mac-Low, M. M., Van Buren, D., Wood, D.O.S., & Churchwell, E., ApJ, 369 395

Serabyn, J?., Lacy, J.H., Achtermann, J. M., 1992, ApJ, 395, 166

Soker, N., 1990, ApJ, 358, 545

Soker, N., 1991, ApJ, 376, 750

Van Buren, D., 1986, ApJ, 306, 358

Van Buren, D. & McCray, R. 1988, ApJ, 329, L93

Van Buren, D., Mac-Low, M. M., Wood, 11.0. S., Churchwell, E. 1990, ApJ, 353, 570

Vishniac, E.T., 1994, ApJ, 428, 186

Yusef-Zadeh, F., & Melia, F. 1992, ApJ, 385, L 41

TABLE 1

The parameters characterizing the four runs

| | model A | model B | model C | model D | model E |
|---|---|---|---|---|---|
| $v_*/v_w$ | 1 | 1 | 1 | 2 | 0.5 |
| $\Delta R$ | 0.02 | 0.02 | 0.04 | 0.02 | 0.02 |
| At | 3.3 x 10-$^{3}$ | 3.3 x 10-$^{3}$ | 6.6 × 10-$^{3}$ | 1.6 × $10^{-3}$ | 3.3 × $10^{-3}$ |
| $N_{in_j}$ | 288 | 576 | 288 | 288 | 288 |

## FIGURE CAPTIONS

Fig. 1: The geometry and the coordinate system are shown.

Fig. 2: The surface density for model A. In the last panel all the previous panels are plotted together.

Fig. 3: Gray scale space versus time plot for the surface density of model A. The horizontal axis is the z projection of the coordinate along the 1 ow shock.

Fig. 4: The surface density for model B.

Fig. 5: The surface density for model C.

Fig. G: Diagram of the relationship between the instability growth rate, C(1), as derived from the linear analysis of paper I, versus $v_*/v_w$ for 1 = 1.

Fig. 7: The time averaged relative perturbations in 1 he surface density for models D and E.

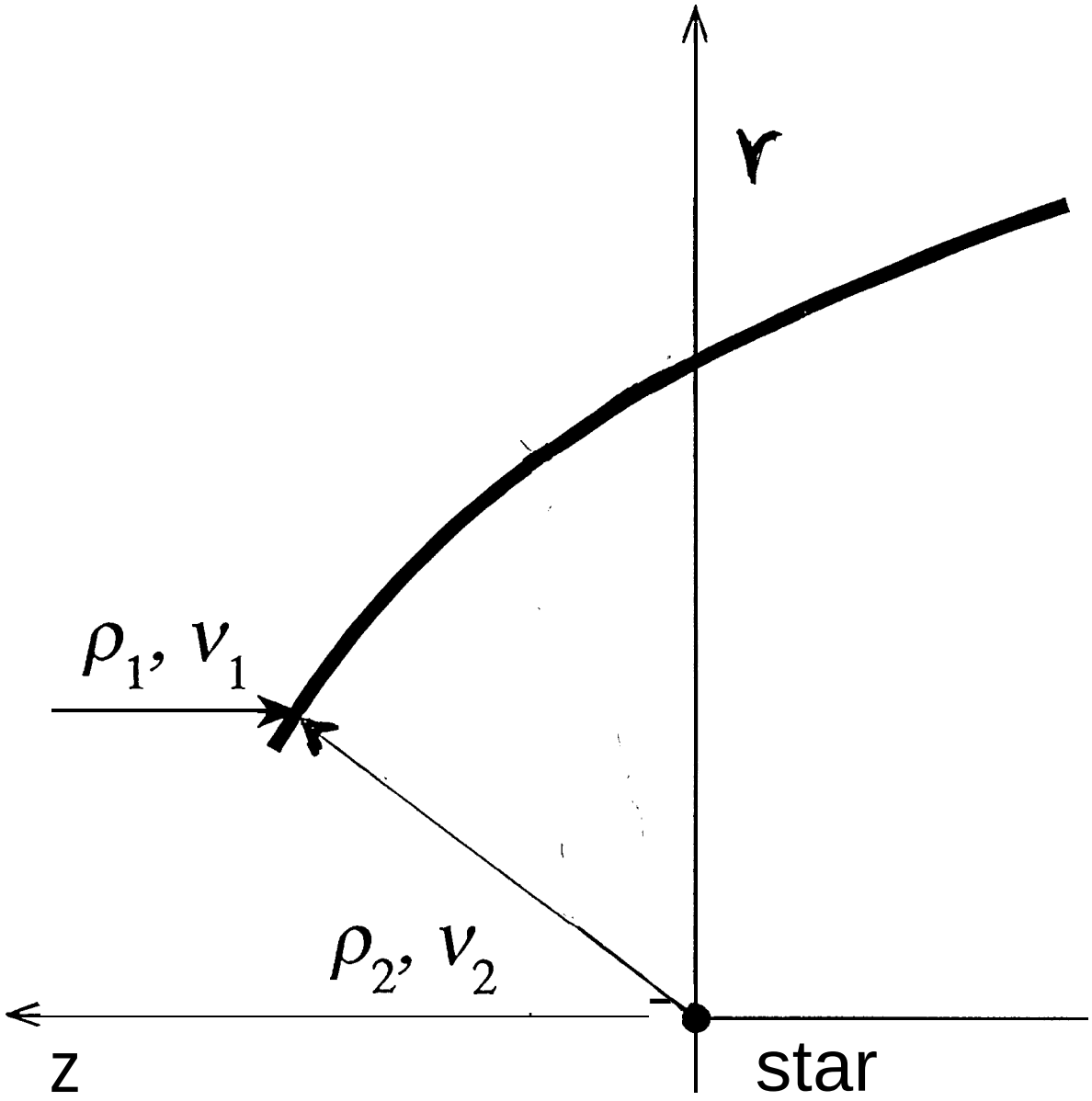


Fig. 1

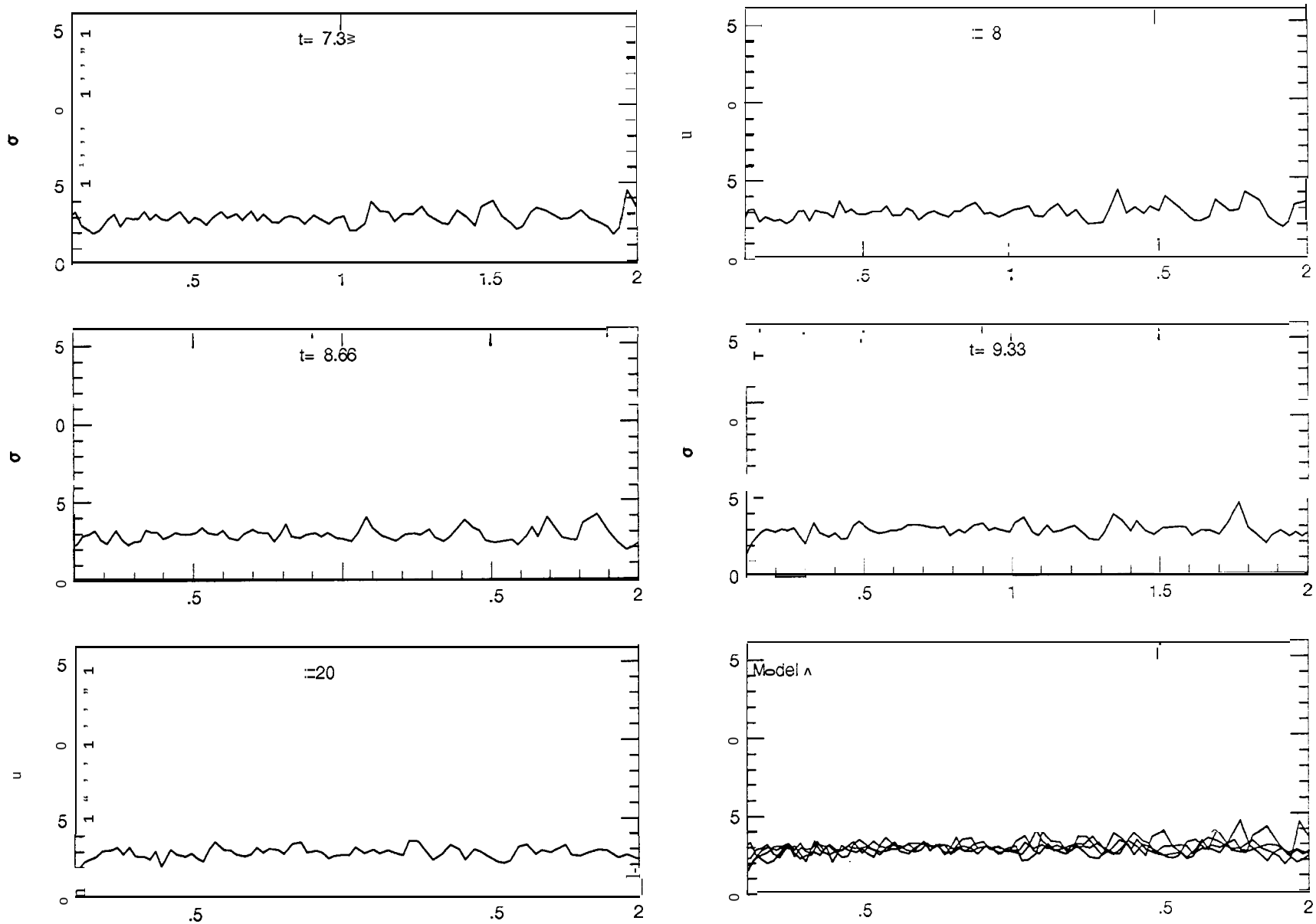
t= 7.33
t= 8
t= 8.66
t= 9.33
:=20
Model ∧
σ
u
0
5
.5
1
1.5
2

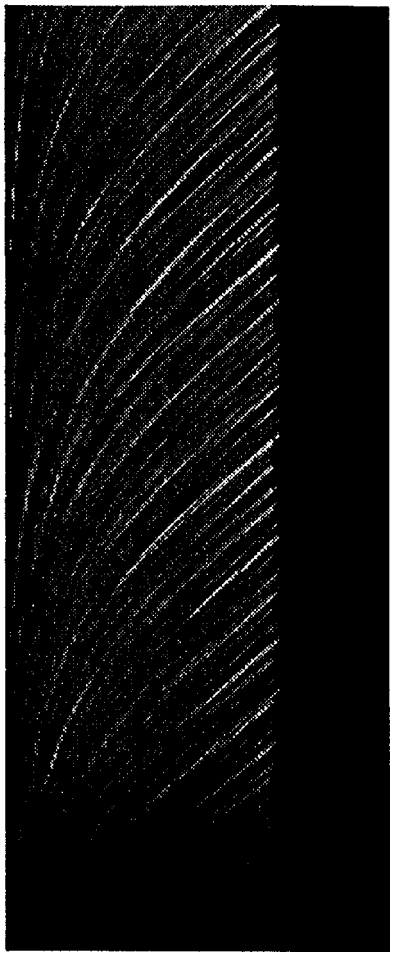

Fig. 3

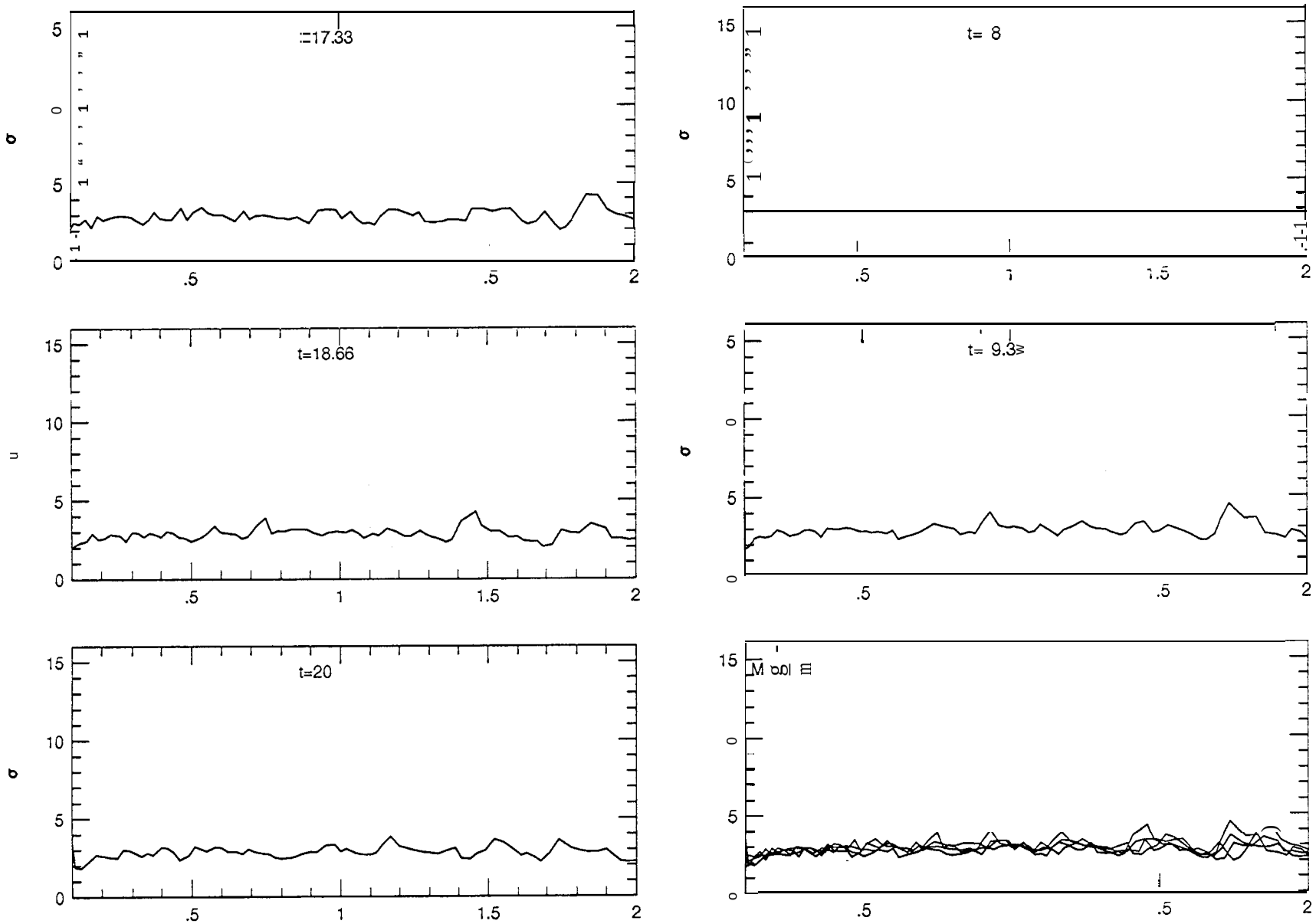


Fig. 4

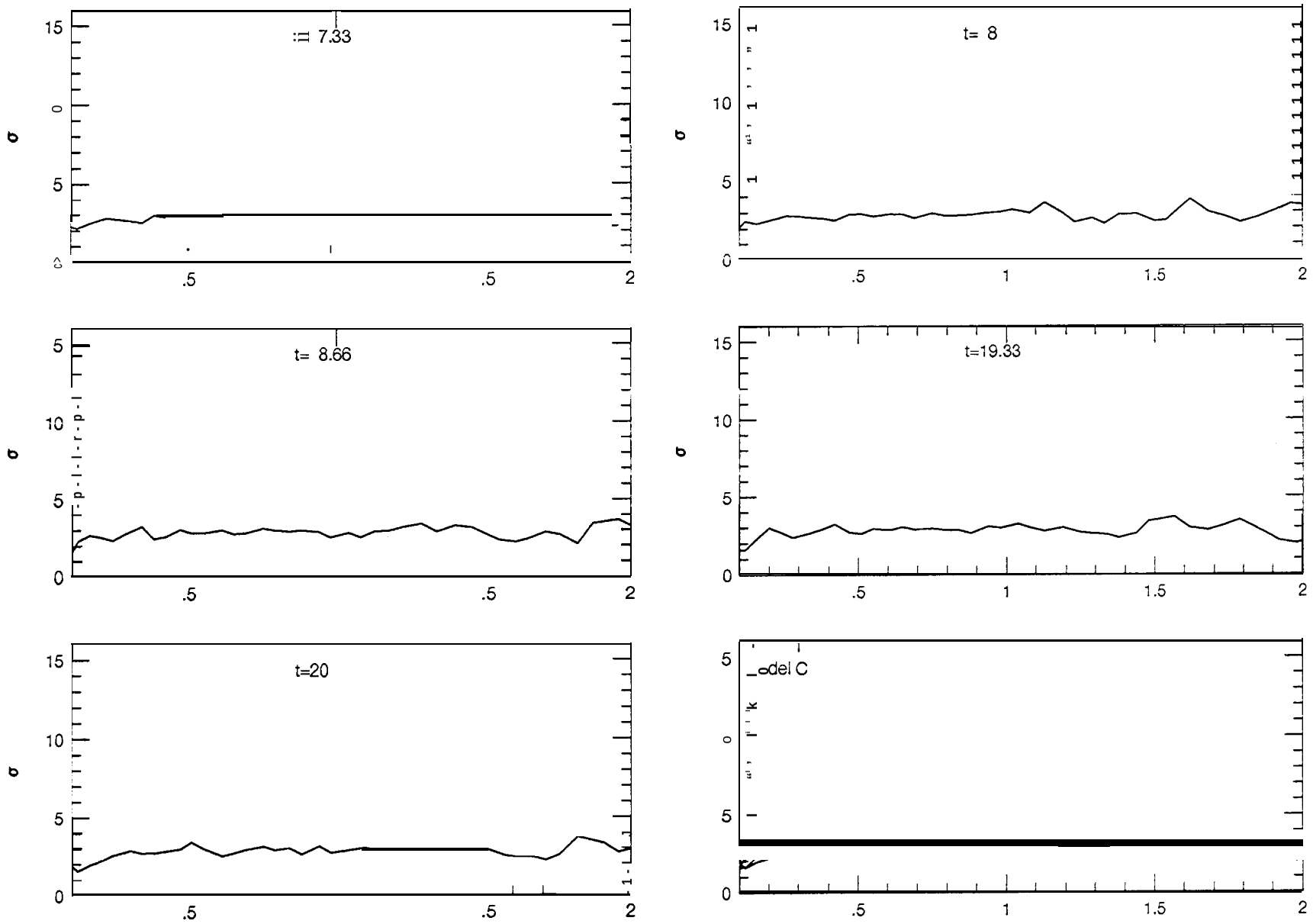


Fig 5

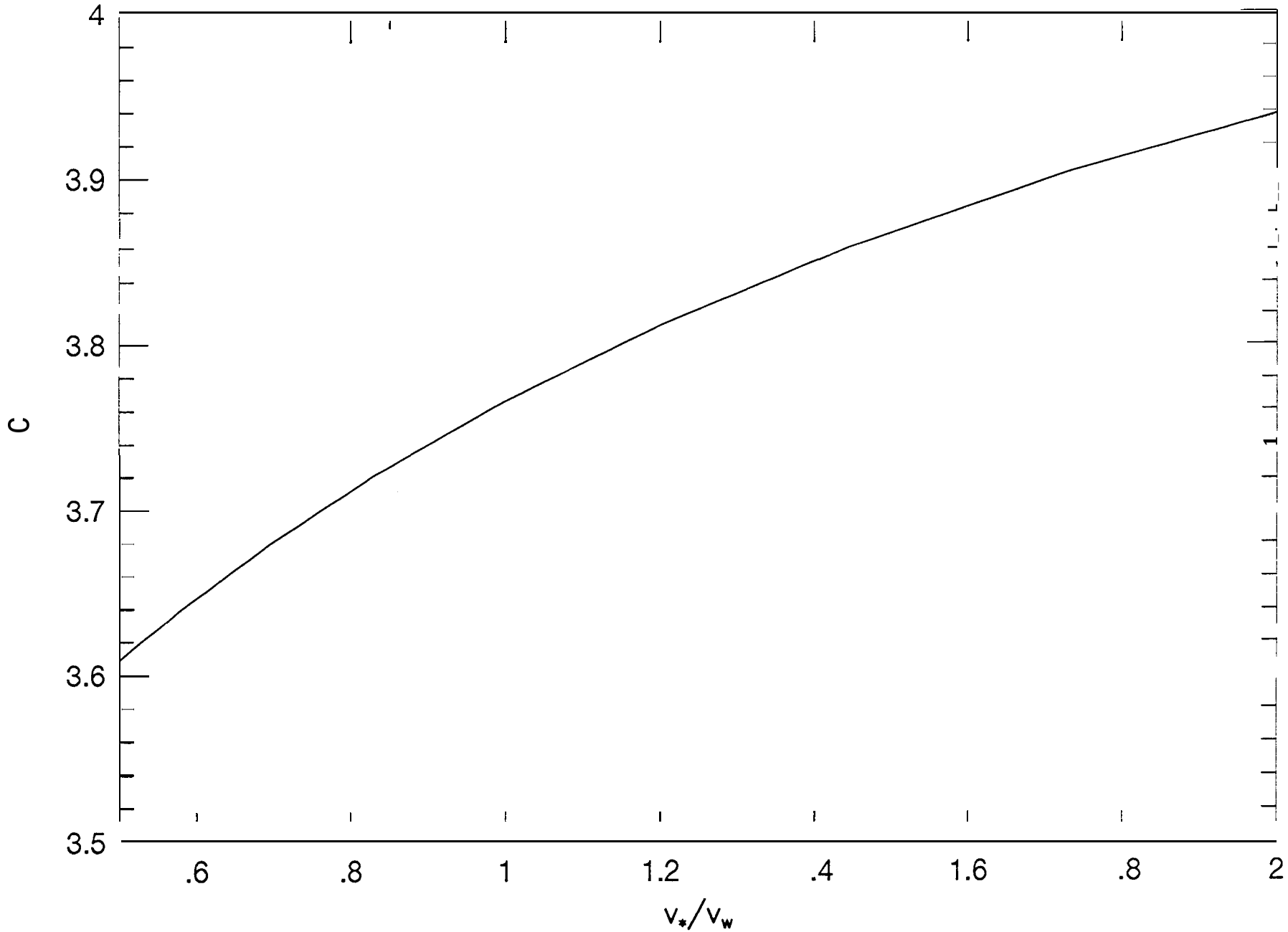


Fig. 6

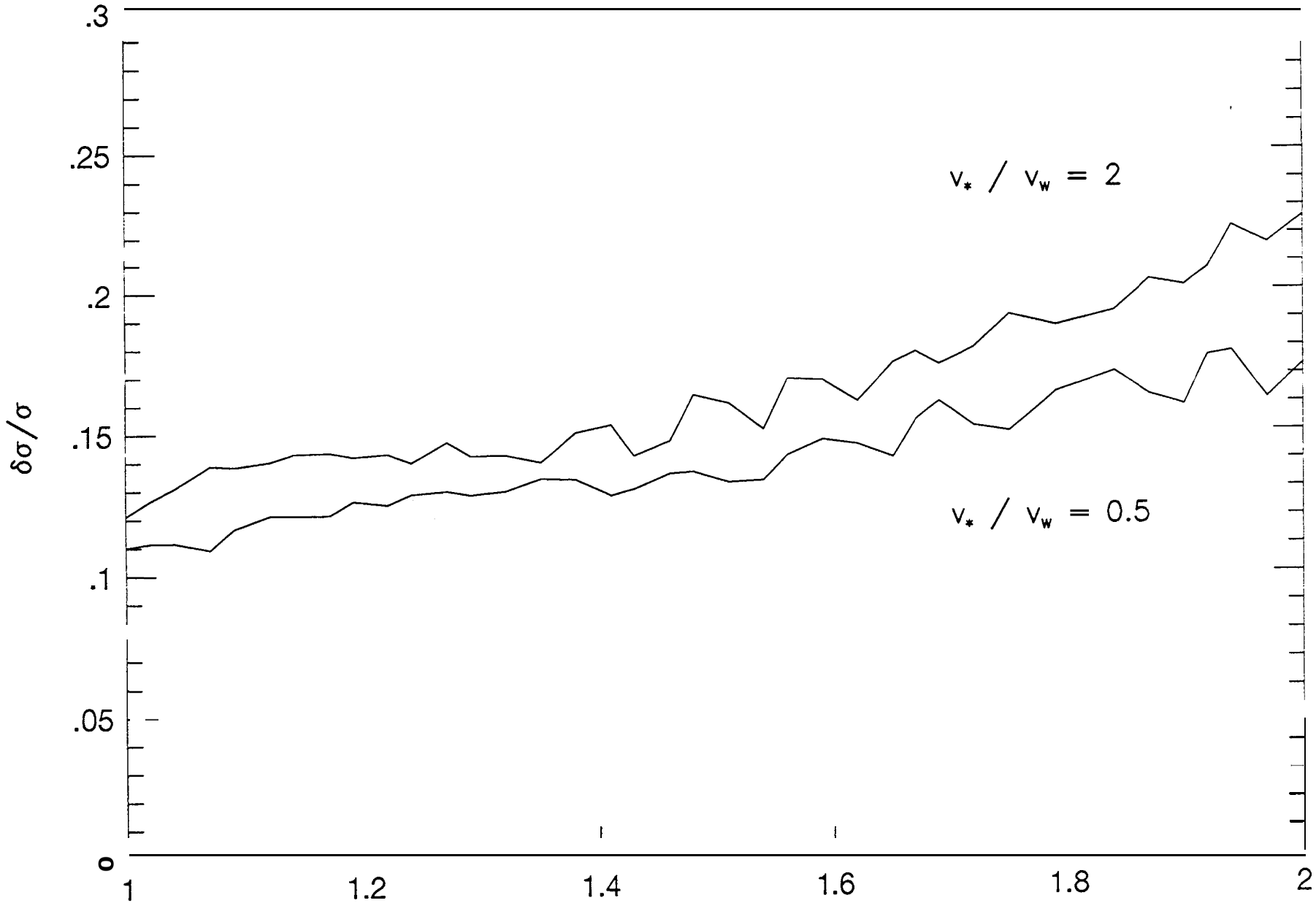


Fig. 7